

Fabrication of 3D nanostructures by multidirectional UV lithography and predictive structural modeling

This content has been downloaded from IOPscience. Please scroll down to see the full text.

2015 J. Micromech. Microeng. 25 025017

(<http://iopscience.iop.org/0960-1317/25/2/025017>)

View [the table of contents for this issue](#), or go to the [journal homepage](#) for more

Download details:

This content was downloaded by: kjungkwun

IP Address: 158.130.80.14

This content was downloaded on 19/05/2015 at 19:42

Please note that [terms and conditions apply](#).

Fabrication of 3D nanostructures by multidirectional UV lithography and predictive structural modeling

Jungkwun Kim¹, Cheolbok Kim², Mark G Allen¹ and Yong-Kyu 'YK' Yoon^{2,3}

¹ University of Pennsylvania, Philadelphia, PA, USA

² University of Florida, Gainesville, FL, USA

E-mail: ykyoon@ece.ufl.edu

Received 29 July 2014, revised 27 October 2014

Accepted for publication 7 November 2014

Published 22 January 2015



Abstract

This paper presents the fabrication and modeling of three-dimensional (3D) nanostructures by automated multidirectional ultraviolet (UV) lithography, which is a fast, cost-effective, manufacturable fabrication method. Multidirectional UV exposure is performed using a static UV light source equipped with a tilt-rotational substrate holder. A glass substrate with a nanopatterned chrome layer is utilized as both a photomask and a substrate, for which a backside UV exposure scheme is used. For the analytical modeling of the shape of fabricated nanostructures, UV exposure dosage, diffraction and refraction effects, and absorption rate are taken into account. For more accurate process predictive models, a commercially available multiphysics simulation tool is used. The structural shapes predicted from analytical calculation and simulation are compared with the fabricated ones for which various 3D nanoscale test structures are fabricated such as an inclined nanopillar array and a vertical triangular slab. Also, nanostructures with multiple heights are successfully implemented from single layer photoresist by controlling the UV exposure dosage and tilt angles. A tripod embedded horn and a triangular-slab embedded horn are demonstrated.

Keywords: 3D nanostructures, multidirectional UV lithography, SU8

(Some figures may appear in colour only in the online journal)

1. Introduction

Development of three-dimensional (3D) 'nano' and submicron scale device architectures and fabrication processes has emerged as important framework for numerous applications in optical, bio, and radio frequency (RF) fields. Recent studies show various nanoscale structures for energy harvesting devices [1, 2], scaffolds for tissue engineering [3, 4], plasmonic structures [5, 6], and optical devices [7–9]. However, some fabrication methods for 3D nanostructures require expensive equipment and/or laborious and time consuming process steps such as x-ray lithography [10], laser lithography including two-photon [11], multi-photon [12] or interference lithography [13], and electron beam lithography

[14]. The 3D printing process becomes popular as an economic prototyping method while the nature of its serial process usually requires lengthy process time holding limitations in manufacturability.

Meantime, simple, cost-effective, manufacturable alternatives in nanofabrication, such as nano imprinting [15], hot embossing [16], and polydimethylsiloxane (PDMS) molding [17] have been explored. These fabrication methods enable multiple copies of nano structures to be produced with minimal damage to the original master structure. However, the fabricated geometries are restricted to the shapes which are easily moldable and demoldable from the parent structures. Any geometry with a bridge or closed loop structure may not be reproducible from these approaches.

Dynamic mode multidirectional UV lithography (DMUL) has been introduced for 3D microfabrication where the

³ Author to whom any correspondence should be addressed.

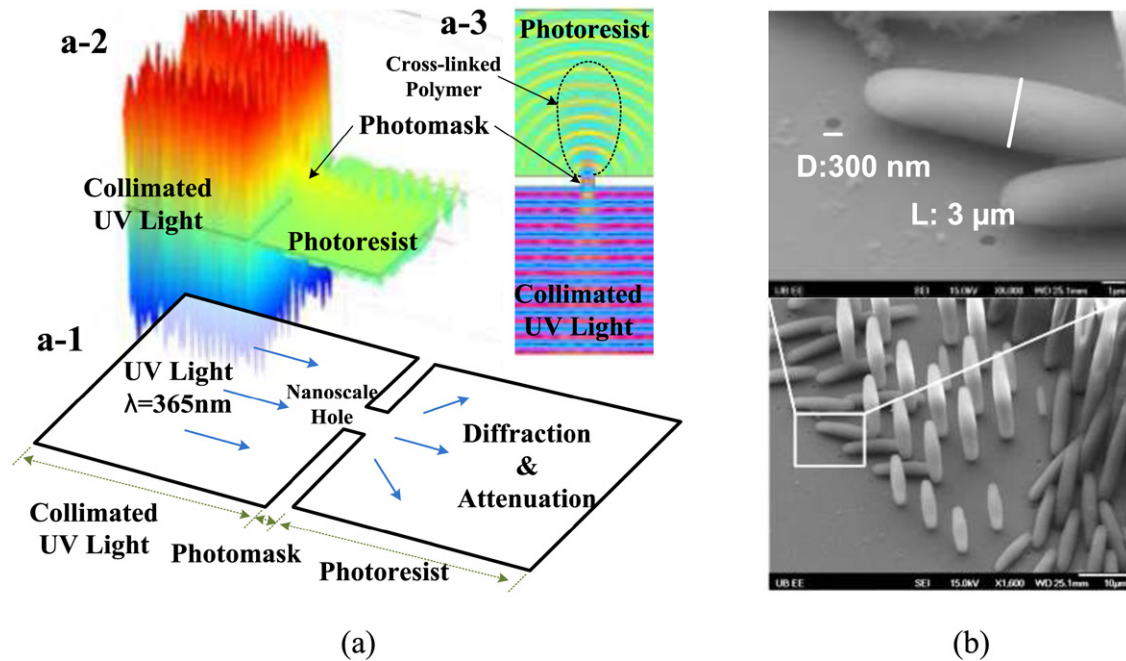


Figure 1. Submicron UV lithography: (a) UV exposure through a nanoscale subwavelength pattern in schematic diagram (a-1), 3D simulation plot (a-2), and top view of 2D simulation plot (a-3), (b) fabricated submicron pillar array and nanohole mask (enlarged view).

substrate holder under UV light exposure has tilt and rotational movements as preprogrammed or interactively to create multiple UV light traces through photomask patterns, enabling to form complex latent 3D images [18]. After post-exposure bake and developing processes, the latent 3D images are transformed to 3D structures. DMUL is advantageous since the fabrication process is straightforward, economic, and mass producible as the conventional UV lithography process, and moreover the resultant structures from the DMUL process are not limited to the original photomask pattern but able to produce an unlimited number of 3D structures. Various microstructures such as inclined pillars, triangular plates, cardiac-shape horns, and screwed wind vanes with double and quadruple blades have been demonstrated [18]. However most fabricated structures by DMUL have been demonstrated in micron to millimeter scale, and the fabrication capability of DMUL has not been investigated in nano/submicron ranges where optical interferences such as diffraction, refraction, and absorption would affect more significantly.

In this paper, 3D fabrication capability of the DMUL process has been explored in nano/submicron resolution. Photopatternable epoxy SU8 (Microchem Inc.) is used as photoresist and is applied on a glass substrate with nano/submicron scale photomask patterns. The glass substrate serves both a substrate and a photomask and DMUL is performed with a backside UV exposure scheme. As the dimension of the photomask patterns is in the similar range of the wavelength of the UV light source, there are severe UV diffraction or scattering effects in ray tracing, which would have been minimally considered in UV patterning with micro/millimeter scale photomask patterns. Analytical solutions and numerical simulations are used to predict 3D ray tracing patterns with various applied UV exposure dosages. Predicted

3D nanostructure dimensions are compared with those of the fabricated 3D nanostructures.

2. Concept and modeling

When a light or electromagnetic wave encounters a blocking obstacle, diffraction occurs at the edge of the blocking object. In photolithography, it is the boundary between the dark and clear fields of a photomask pattern that experiences major diffraction. The influence of the diffraction effect in patterning increases when the wave propagates in a medium with a different refractive index after the photomask. If an air gap exists between the photomask and the photoresist, the diffracted wave after the photomask also experiences refraction due to the difference of the refractive indices between the photomask (glass or quartz) and air, resulting in enlarged boundary regions and degraded patterning resolution. As the refractive index difference between the photomask and photoresist is usually smaller than the difference between the photomask and air, getting rid of the air gap can mitigate the degradation of the patterning resolution. In practice, often the backside UV exposure scheme is adopted for the zero air gap, where photoresist is directly dispensed on the photomask, which serves as a substrate as well. Light is exposed through the photoresist and the wave propagates from the photomask to the photoresist. Also, it should be noticed that the diffraction effect becomes prominent when the opening size of the photomask pattern is similar to or smaller than the wavelength of the UV light source. Figure 1 describes the backside exposure scheme where a collimated UV light with a wavelength of 365 nm (*i*-line) incidents through an opening whose dimension is 300 nm. Figure 1(a-1) shows the schematic of a 2D simulation setup. The waveform has been simulated using

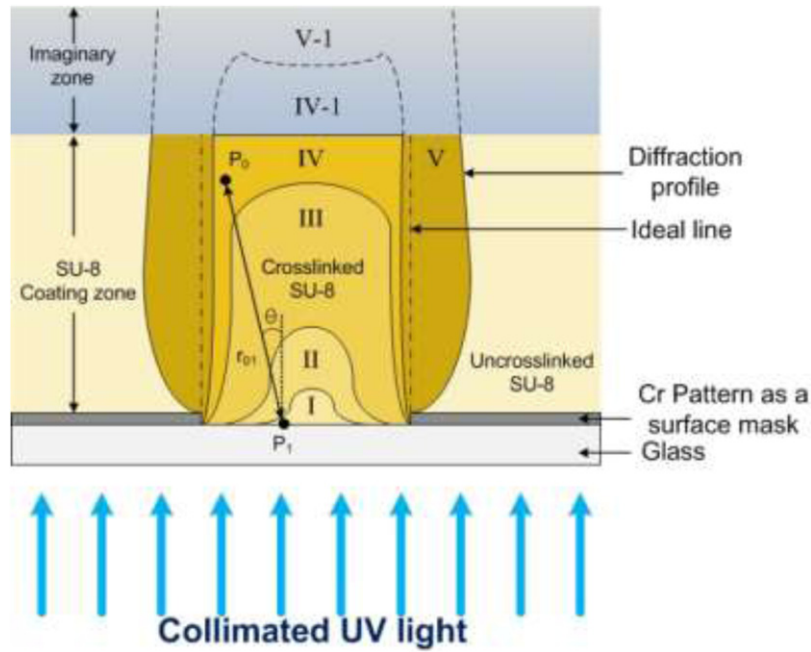


Figure 2. Schematic diagram of backside UV exposure with a submicron photomask pattern: (I–III) SU8 growing region, (IV) ideal SU8 crosslink, (V) SU8 crosslink from diffracted light, (IV–1, V–1) imaginary zone; light propagates after the photoresist.

a finite element multiphysics simulation tool (Multiphysics module: wave propagation, COMSOL Inc.) as shown in figure 1(a-2). The simulation result shows that the collimated wavefronts are transformed to the spherical ones after passing the photomask opening due to diffraction. As the height of the waveform indicates the wave intensity, it is observed that the intensity is markedly decreased in the photoresist region after the photomask opening. If the optical dosage, which is the intensity times the exposure time, exceeds the minimum cross-linking level for a negative tone photoresist, the pattern is likely to remain after development. Assuming the same exposure time is applied, an equi-dosage line can be drawn using the dashed line as shown in figure 1(a-3), forming an ellipsoidal boundary. To verify the shape, an SU8 pillar array has been fabricated using a photomask consisting of an opening array with an opening diameter of 300 nm as shown in figure 1(b) following a typical UV lithography process. The applied optical dosage is more than 10 times the crosslinking dosage. Many pillars are collapsed due to the large pillar body size compared to the anchoring point whose dimension is approximately 300 nm. However, the ellipsoidal profiles of the fabricated pillars are clearly observed as predicted. The shape is qualitatively in good agreement with the simulated one.

For more conceptual analysis, experiments with different optical dosages to photoresist are performed and the resultant geometries can be examined. Patterned geometry is categorized in 5 different cases I–V as shown in figure 2. In case I–III, the optical dosage is not sufficient to crosslink the photoresist in its full thickness. The size of crosslinked photoresist increases as applied UV dosage increases. In case IV, the applied UV dosage is sufficient to crosslink the photoresist in its full thickness. An excess amount of UV dosage can be applied to outside the photoresist, where air presides and can be called as an imaginary zone. In this case, the height of the

fabricated structure is limited by the thickness of the photoresist and the width can be smaller or bigger depending on the magnitude of diffracted optical dosage. Case V shows a case when a large amount of the diffracted optical dosage causes the width to be larger than the mask opening size.

For more rigorous quantification, optical ray trace in subwavelength UV lithography is analytically studied by incorporating Rayleigh–Sommerfeld diffraction formulation and a numerical analysis of Fresnel–Kirchhoff diffraction model [19]. Overall, the effects of diffraction, intensity of the UV light, transparency of the photoresist (optical absorption), and the refraction effect occurred in the interface of different refractive index media are taken into account. Note that the air gap effects are not considered as the backside UV exposure process is used. The electric field U of the Rayleigh–Sommerfeld equation at a position P_0 in the SU8 medium is induced by the light propagation governed by the Fresnel–Kirchhoff diffraction equation and the light-intensity I is derived from the electric fields U as expressed in the following equations.

$$U(P_0) = \frac{1}{j\lambda} \iint_{\Sigma} U(P_1) \frac{\exp(jkr_{01})}{r_{01}} \cos \theta ds \quad (1)$$

$$I(P_0) = \frac{1}{2\eta_0} |n_{\text{SU-8}} \cdot U(P_0)|^2 \quad (2)$$

where $U(P_1)$ is the amplitude of the incident collimated light wave on the mask (point P_1) as indicated in figure 2. λ , k , η_0 and n_{SU8} are the wavelength (365 nm) of UV light, the wave number, intrinsic impedance in air (377Ω) and the refractive index of photoresist (SU8 = 1.67 for i -line [18]), respectively. The r_{01} and θ are the distance and the angle between P_0 and P_1 , respectively. $I(P_0)$ is the UV light intensity at the position of P_0 in the SU8 medium.

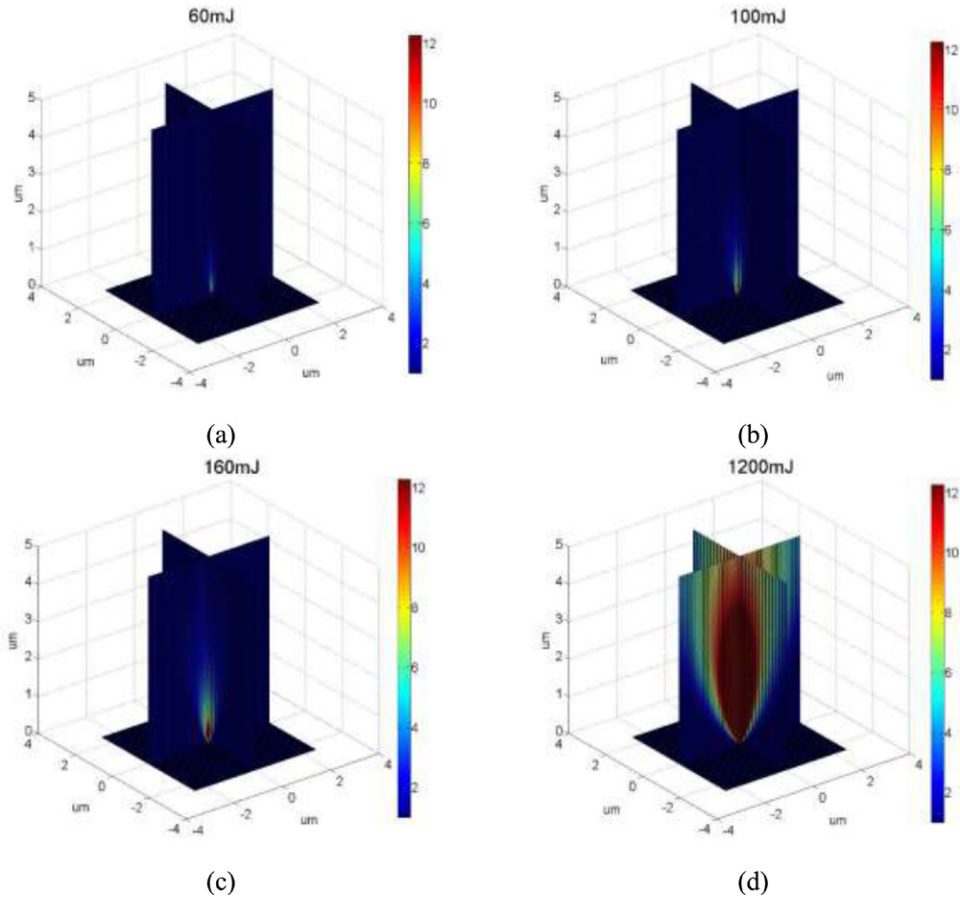


Figure 3. UV exposure dose distribution with different applied dosages: (a) 60mJ cm^{-2} , (b) 100mJ cm^{-2} , (c) 160mJ cm^{-2} , and (d) 1200mJ cm^{-2} .

The distribution of dosage D in SU8 can be calculated by the following equations [20], considering the absorption coefficient of photoresist.

$$D(P_0, t_{\text{exp}}) = \frac{(1 - R_1)(1 - R_2)I(P_0)t_{\text{exp}}\{\exp(-\alpha_{\text{unexp}}z) - \exp(-\alpha_{\text{exp}}z)\}}{(\alpha_{\text{exp}} - \alpha_{\text{unexp}})z}$$

$$R_1 = 0.5 \left(\left(\frac{n_{\text{air}} / \cos(\delta) - n_{\text{Pyrex}} / \cos(\theta)}{n_{\text{air}} \cos(\delta) + n_{\text{Pyrex}} \cos(\theta)} \right)^2 + \left(\frac{n_{\text{air}} \cos(\delta) - n_{\text{Pyrex}} \cos(\theta)}{n_{\text{air}} \cos(\delta) + n_{\text{Pyrex}} \cos(\theta)} \right)^2 \right)$$

$$R_2 = 0.5 \left(\left(\frac{n_{\text{Pyrex}} / \cos(\delta) - n_{\text{SU8}} / \cos(\theta)}{n_{\text{Pyrex}} \cos(\delta) + n_{\text{SU8}} \cos(\theta)} \right)^2 + \left(\frac{n_{\text{Pyrex}} \cos(\delta) - n_{\text{SU8}} \cos(\theta)}{n_{\text{Pyrex}} \cos(\delta) + n_{\text{SU8}} \cos(\theta)} \right)^2 \right) \quad (3)$$

where R_1 is the reflection coefficient between the air and glass and R_2 is the reflection coefficient between the glass and photoresist. δ and θ are the incident and refracted angles of the UV light at the boundaries, respectively [20]. n_{air} and n_{Pyrex} are the

refractive index of air (1 for *i*-line), Pyrex glass wafer (1.47 for *i*-line [21]), respectively. t_{exp} is the exposure time. And α_{exp} and α_{unexp} are the UV absorption coefficient ($49 \pm 1\text{ cm}^{-1}$ and $38 \pm 1\text{ cm}^{-1}$) of the exposed and unexposed photoresist (SU8) for *i*-line, respectively [21]. If the applied dosage is larger than the critical one (or crosslinking dosage) of photoresist (SU8), polymerization occurs after post-exposure baking.

UV exposure dosage is calculated with a photomask opening diameter of 300 nm and an SU8 thickness of $5\mu\text{m}$. The minimum SU8 crosslinking dosage used is 12mJ cm^{-2} . Applied dosages of 60, 100, 160 and 1200mJ cm^{-2} result in a calculated height of 160, 500, 870, 5000nm as shown in figures 3(a)–(d), respectively. In this calculation, process parameters associated with development and solvent swelling effects are not considered.

To verify the calculated geometrical dimension, SU8 pillars have been fabricated as shown in figure 4. A glass photomask with 300 nm circular patterns is spincoated with SU8. Four different SU8 samples with a UV exposure dosage of 60, 100, 160, 1200mJ cm^{-2} have been prepared. Post UV exposure processes have been identical for all the samples: post-exposure bake at 95°C for 60s, development in propylene glycol monomethyl ether acetate (PGMEA) for 60s in room temperature, and rinsing and cleaning with isopropylalcohol (IPA) and deionized (DI) water. The fabricated nanostructures are metalized with 10 nm thick chromium (Cr)

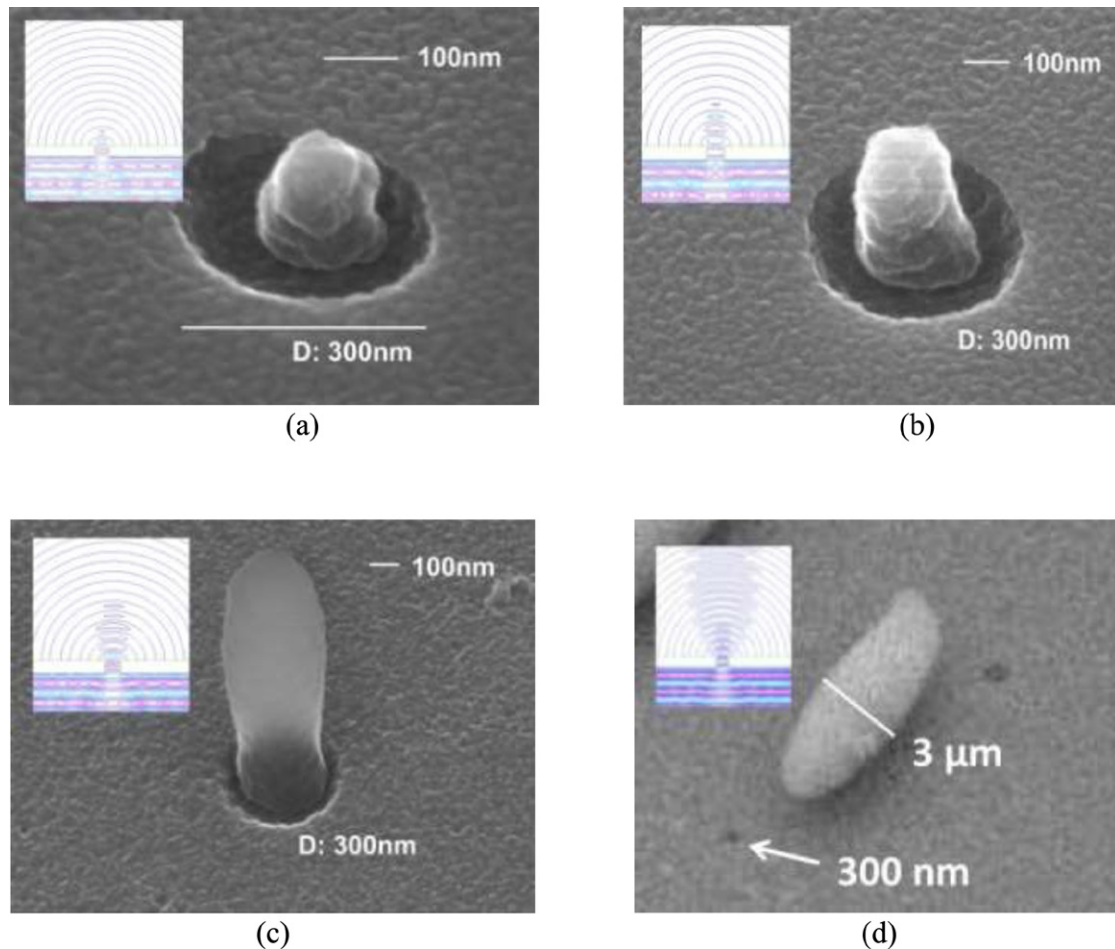


Figure 4. UV lithography through a nanoscale photomask pattern with various optical dosages (inset shows associated simulation by COMSOL): (a) 60 mJ cm^{-2} , (b) 100 mJ cm^{-2} , (c) 160 mJ cm^{-2} , (d) 1200 mJ cm^{-2} .

for scanning electron microscope (SEM) imaging. The fabricated SU8 structures are shown in figure 4 with insets showing 2D ray trace patterns by the wave propagation module of COMSOL. Figure 4(a) shows a pillar diameter of 150 nm and a pillar height of 160 nm fabricated with an optical dosage of 60 mJ cm^{-2} . Note that the pillar diameter of 150 nm is much smaller than the mask pattern diameter of 300 nm due to lack of the optical dosage. Figure 4(b) shows a pillar diameter of 200 nm and a pillar height of 460 nm with 100 mJ cm^{-2} . Note that it shows a tapered sidewall. Still, the fabricated SU8 pillar has a width smaller than the mask pattern width of 300 nm. Figure 4(c) shows an average pillar width of 300 nm and a pillar height of 810 nm with 160 mJ cm^{-2} . The sidewall is not straight but curvy. Figure 4(d) shows an average pillar diameter of $3 \mu\text{m}$ and a height of approximately $6 \mu\text{m}$ with a UV dosage of 1200 mJ cm^{-2} . Note that this sample starts with an initial SU8 thickness of $10 \mu\text{m}$. The fabricated pillar structures show significantly 'swollen' shapes compared with the mask pattern and mostly fall down after development due to the small foot print supporting the large body. Fabricated SU8 structures in figure 4 show good co-relationship with the calculated ones shown in figure 3.

Figure 5 summarizes the height of the SU8 pillar structures on the 300 nm photomask pattern as a function of

applied UV exposure dosage. The calculated heights and the experimentally obtained ones are compared. No pillar structure is formed for the UV exposure dosage below 12 mJ cm^{-2} which is described as the 'uncrosslinked' zone. Polymerized SU8 pillars are observed in the 'growing' zone and the height of the pillars increases as UV dosage increases. For the excessive UV exposure experiment, a $10 \mu\text{m}$ SU8 layer has been used for experiments. Pillars with a pillar height of $6 \mu\text{m}$ and an average diameter of $3 \mu\text{m}$ have been obtained.

3. Fabrication process of nano DMUL

The fabrication sequence of the nano DMUL process is described in figure 6. A photomask comprising various circular patterns with diameters of 100 nm–900 nm is prepared on a Chromium (Cr) coated glass substrate (Chrome photomask black, TELIC) as shown in figure 6(a). E-beam lithography was used for patterning the nano scale aperture. The Cr-coated glass was cleaned using Trichloroethylene (TCE), Acetone, and Methanol followed by Deionized water rinse. After drying the substrate, the Cr-coated surface is spin-coated with polymethyl methacrylate (PMMA).

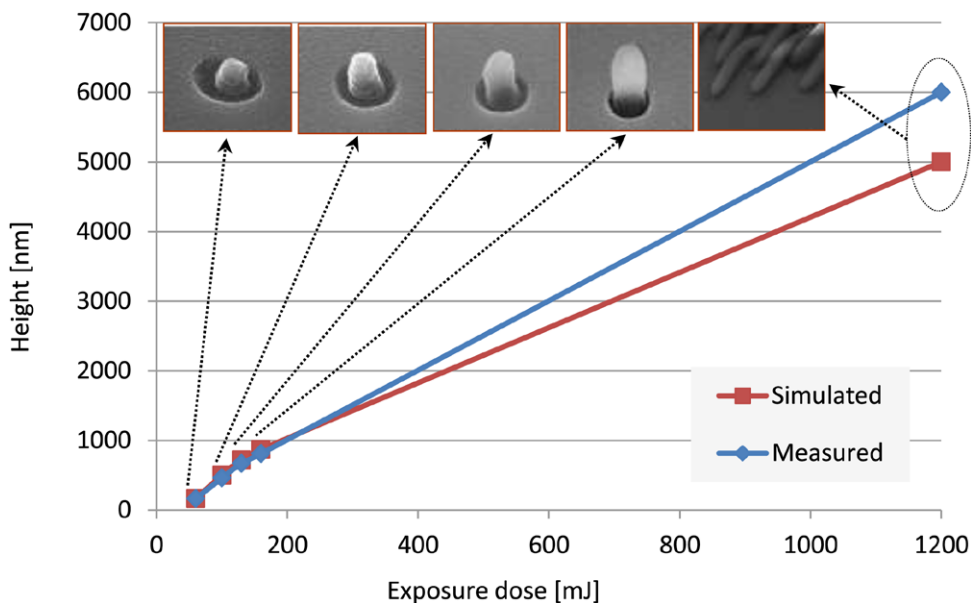


Figure 5. UV energy on SU8 structures versus height.

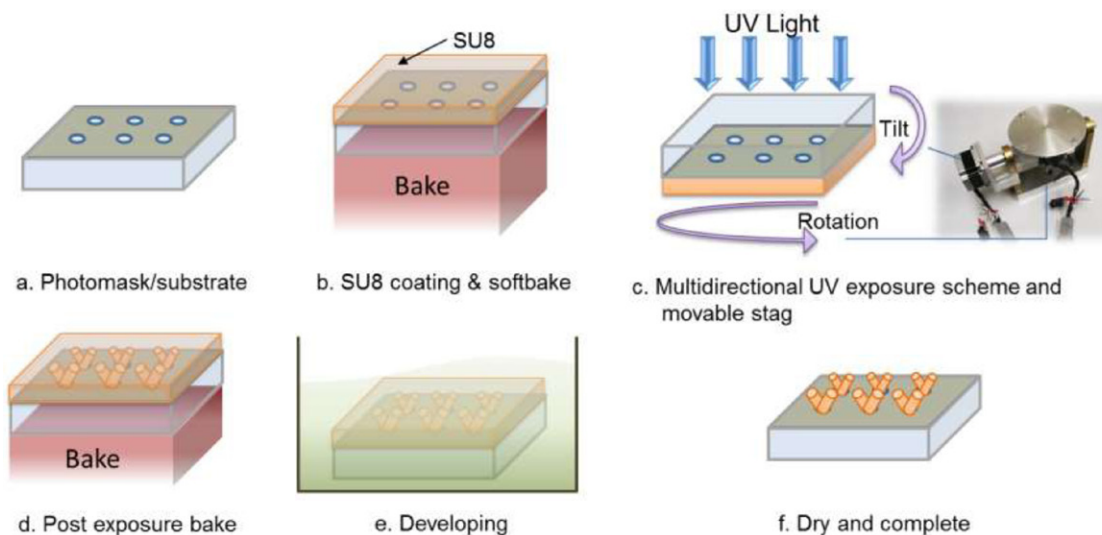


Figure 6. NanoDMUL Fabrication process.

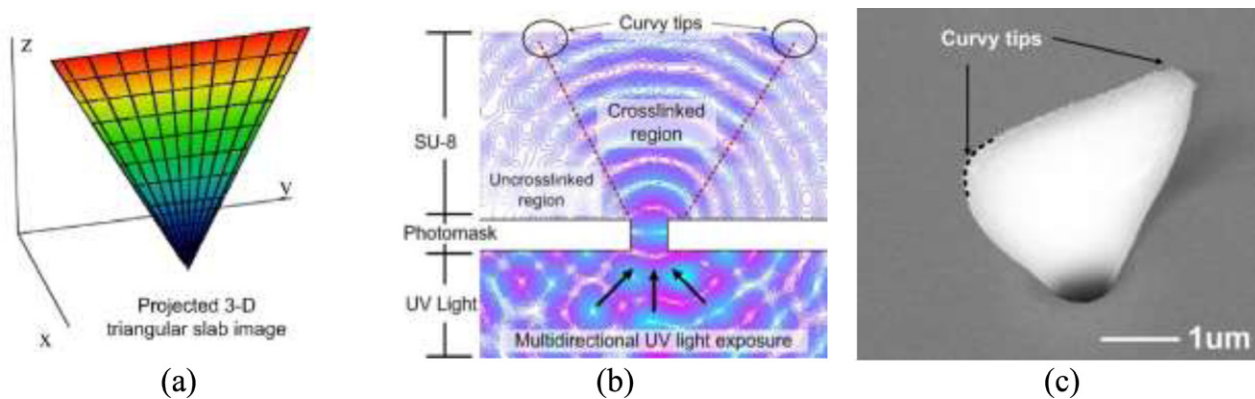


Figure 7. Design, simulation, and fabrication of a triangular slab: (a) the ray trace skeleton of UV light, (b) 2D simulation results, (c) a fabricated triangular slab.

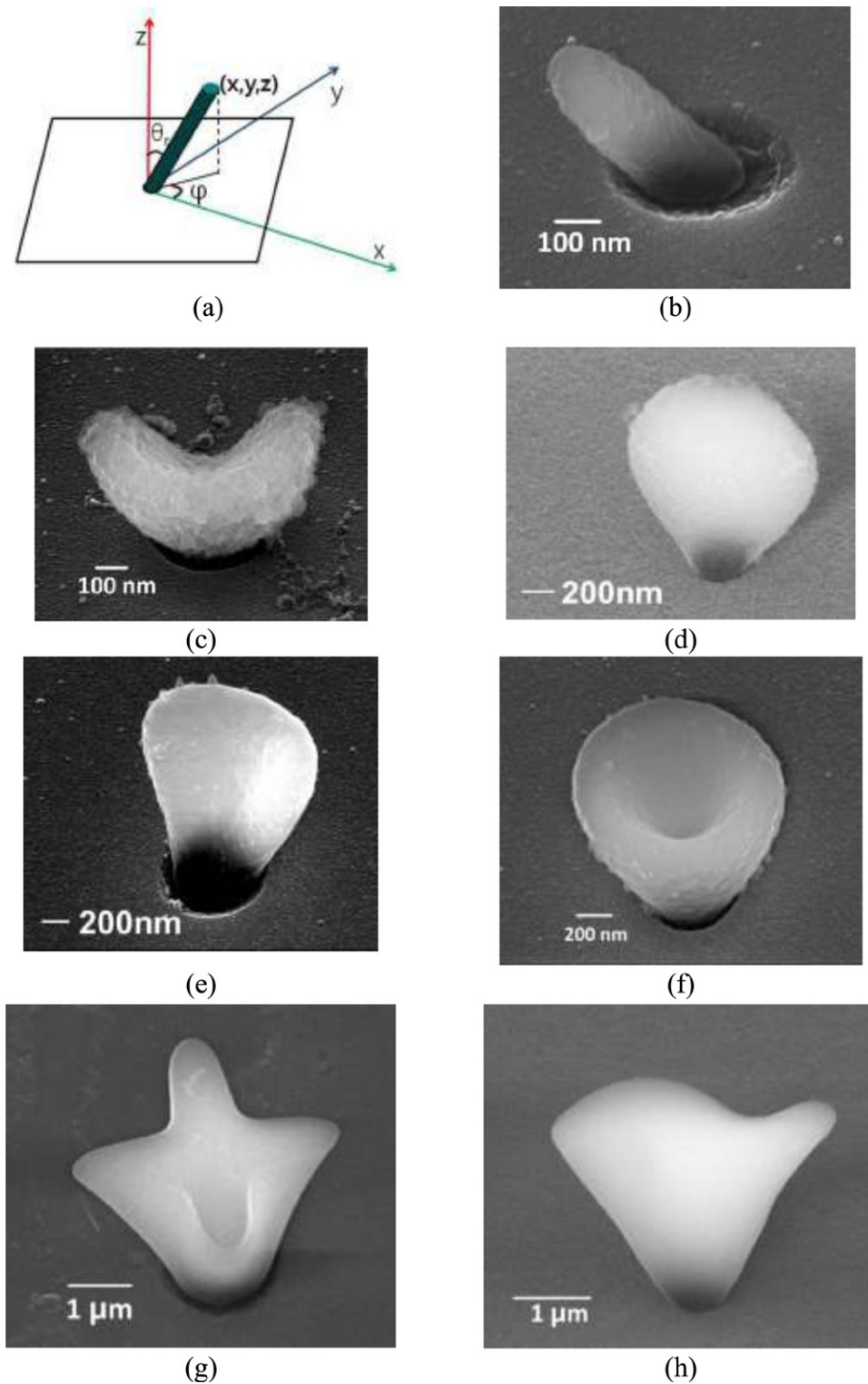


Figure 8. Fabricated 3D nanoscale structures, (a) spherical coordinate system used to explain multidirectional UV light trace, (b) an inclined nanopillar, (c) a ‘V’ shape nanopillar, (d) a fan shape nanostructure, (e) a leaf shape nanostructure, (f) a horn shape nanostructure, (g) a quadruple blade, (h) a screwed blade.

An E-beam tool (6500F, Joel Inc.) is used to form an array of nano scale apertures. The substrate is developed (Methyl isobutyl ketone) and rinsed, followed by Cr etching (Ceric ammonium nitrate). The remaining PMMA is removed. Since the photomask serves as a substrate for UV backside exposure, SU8-2005 (MicroChem Inc.) is dispensed on the mask

substrate and spin-coated at 3000 rpm for 30 s and followed by softbaking at 95 °C for 30 s (figure 6(b)). After cooling down to room temperature (22 °C), the sample is placed on the tilt-rotational holder for UV exposure. While the tilt-rotational holder is moving through preprogrammed patterns, the collimated UV light is applied on the sample with the calculated

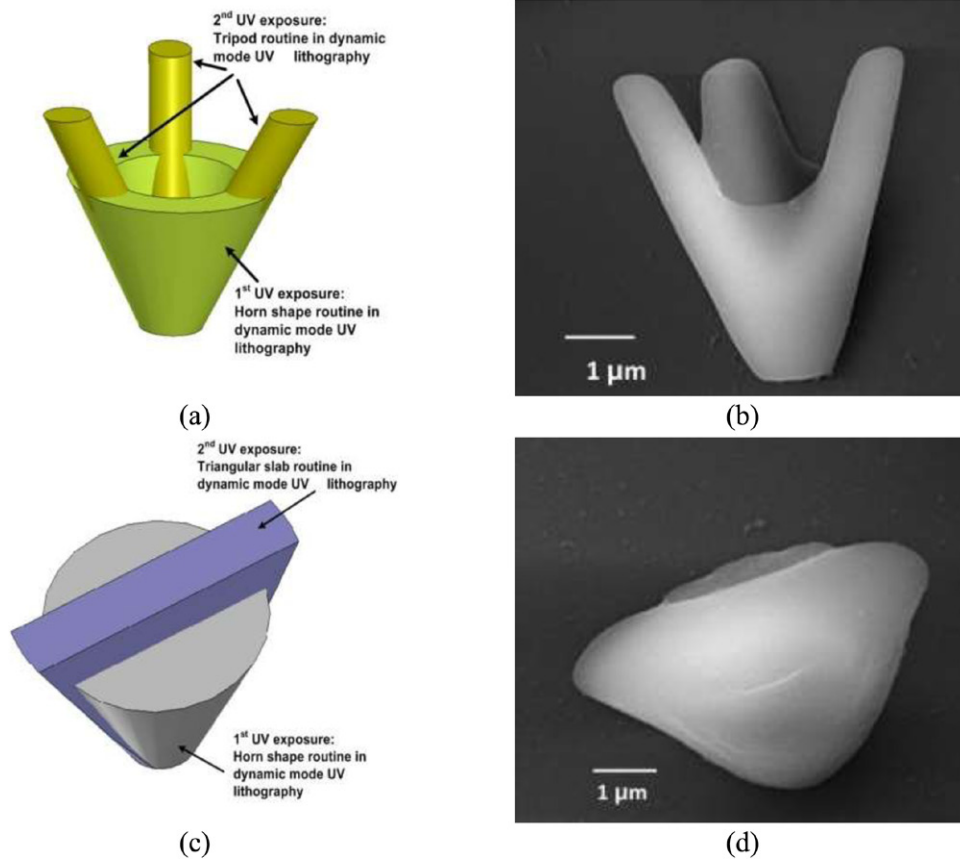


Figure 9. Nano structures implemented by multiple static and dynamic multidirectional UV lithography steps on a single layer of photoresist: (a) a schematic drawing of a horn embedded tripod, (b) a fabricated horn embedded tripod, (c) a schematic of a triangular slab embedded horn, and (d) a fabricated triangular slab embedded horn.

UV exposure dosage (figure 6(c)). After post exposure bake (PEB) at 95 °C for 60 s (figure 6(d)), the sample is developed in PGMEA solution for 60 s (figure 6(e)). Note that no agitation or stirring is performed during the developing process. The sample is rinsed with IPA and DI water, completing the fabrication process (figure 6(f)).

4. Result

Figure 7 shows the design, simulation and fabrication of a submicron scale 3D triangular slab. Figure 7(a) shows the ray trace skeleton of UV light after a scope of tilt motion to form a triangular slab, where refraction is taken into account while diffraction is not [18]. In this calculation, a scope of tiling angle is in the range of -30° to 30° with no rotational movement. Figure 7(b) shows 2D simulation results (COMSOL multiphysics: wave propagation, COMSOL Inc.) with plane wave incidence in multiple tilt angles, where the results shows the superposition of incident waves from different incident angles. The ray trace skeleton predicts the path of the UV light in x - y - z coordinate to control the sample stage motion while the 2D finite element simulation predicts the cross-sectional view of 3D structure with optical effects. Figure 7(c) shows a fabricated triangular slab. The height of the structure is defined by the initial photoresist thickness. It is noticed that both the top

corners of the triangular slab are rounded as predicted in the simulation of figure 7(b).

Figure 8 shows other 3D nanostructures fabricated by the DMUL method. A spherical coordinate system is introduced to describe the trajectory of ray trace by multidirectional UV exposure as shown in figure 8(a). Various rotational angles (φ) and tilt angles (θ) are used to produce complex 3D nanostructures. Figures 8(b) and (c) show examples of static inclined UV exposure where the both rotational and tilt angles are fixed during the exposure process. An inclined nanopillar has been fabricated with 30° tilt angle (figure 8(b)) and a ‘V’ shape nanopillar is fabricated after two static inclined exposure steps with an azimuthal phase angle difference of 180° each other (figure 8(c)). Figure 8(d) shows an example of a structure fabricated with continuous tilt angle changes. The variation of tilt angle in the range of -30° to 30° with a fixed rotational angle of 30° produces a fan shape nanostructure. Figures 8(e) and (f) show examples of structures fabricated with a continuously rotating at fixed tilt angle stage. A leaf shape nanostructure as shown in figure 8(e) is fabricated with rotational angles of $+40^\circ$ to -40° and a fixed tilt angle of 30° . A horn shape nanostructure (figure 8(f)) is fabricated with rotational angles of 0 – 360° and a fixed tilt angle of 30° . Figure 8(g) shows a ‘cross triangular slab’ where the continuously changing tilt angle (-30° to $+30^\circ$) with two static rotational angles at 0° and 90° is used. Figure 8(h) shows a structure fabricated using

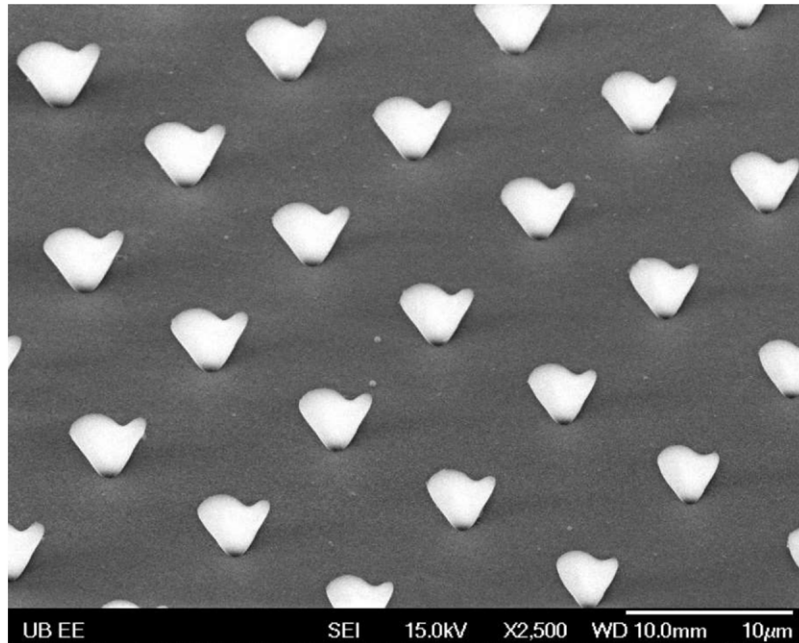


Figure 10. Demonstration of a batch fabricated wind-vane array.

the harmonic combination of tilt and rotational angles. The tilt and rotational angles are ranged in -30° to $+30^\circ$ and -45° to $+45^\circ$, respectively, and these two angles are synchronized. As a result, a ‘wavy triangular slab’ has been fabricated as shown in figure 8(h).

Figure 9 shows nanostructures fabricated using combined dynamic and static multidirectional UV exposure schemes. Figures 9(a) and (c) show the schematics of targeted 3D nanostructures and figures 9(b) and (d) show the corresponding fabricated structures. Figure 9(a) shows an exposure scheme for a horn embedded tripod nanostructure. UV exposure for the horn shape is first performed using dynamic MUL on an SU8 layer followed by static MUL for the tripod shape. UV exposure dosage is higher for the tripod structure, resulting in a relatively taller structure while relatively low dosage is used for the embedded horn structure. A horn embedded tripod nanostructure is successfully fabricated as shown in figure 9(b). Similarly, a UV exposure scheme for a triangular slab embedded horn shape nanostructure is shown in figure 9(c). UV exposure for a horn is performed first using dynamic MUL followed by another dynamic MUL step for a triangular slab. A triangular slab embedded horn is successfully fabricated as shown in figure 9(d).

Figure 10 demonstrates the batch fabrication nature of nanoscale DMUL. An array of fan shape nanostructures are fabricated using a photomask with a 10 by 10 circle array and each circle diameter of 300 nm. The tiling angle for UV exposure is ranged from -30° to $+30^\circ$ and the average height of the fabricated structures is approximately $3\ \mu\text{m}$.

5. Conclusions

The DMUL process has been applied on the submicron photomask pattern for the fabrication of 3D nanostructures. As

diffraction through sub wavelength patterns is significant, a fabricated UV lithography 3D pattern is greatly deformed by diffraction. Ray trace for nano DMUL has been analytically calculated taking into accounts diffraction, refraction, and absorption. Also, fabrication with different optical dosages using a backside exposure scheme has been performed. The fabricated structures show good agreement with the calculated shapes. Also, the shape has been predicted using a commercially available simulation tool. Based on analysis, nano DMUL has been utilized for various 3D nanostructures, where different tilt and rotational angles have been used to show capability to produce various 3D nanostructures. Fabricated 3D nanostructures such as a triangular slab, a screwed wind vane, a quadruple triangular slab, and a horn have been successfully demonstrated. Also, multistep dynamic and static MUL schemes have been exercised for multiple height 3D structures such as a horn embedded tripod structure and a triangular slab embedded horn structure. Different from other sequential nanofabrication processes such as laser patterning and 3D printing, the nano DMUL has batch fabrication capability, which offers low cost manufacturability. This process can be used for nano antennas and frequency selective surfaces as is or with an additional metalization steps in optical, IR, and terahertz ranges.

Author Contributions

The manuscript was written through contributions of all authors. All authors have given approval to the final version of the manuscript.

Acknowledgment

This work has been in part supported by National Science Foundation CMMI 1128806.

References

- [1] Guo W, Xue X, Wang S, Lin C and Wang Z L 2012 An integrated power pack of dye-sensitized solar cell and Li battery based on double-sided TiO₂ nanotube arrays *Nano Lett.* **12** 2520–3
- [2] Qian F, Wang G and Li Y 2010 Solar-driven microbial photoelectrochemical cells with a nanowire photocathode *Nano Lett.* **10** 4686–91
- [3] Kim DH, Lee H, Lee Y K, Nam J M and Levchenko A 2010 Biomimetic nanopatterns as enabling tools for analysis and control of live cells *Adv. Mater.* **22** 4551–66
- [4] Kotov N A *et al* 2009 Nanomaterials for neural interfaces *Adv. Mater.* **21** 3970–4004
- [5] Xu J, Guan P, Kvasnička P, Gong H, Homola J and Yu Q 2011 Light transmission and surface-enhanced raman scattering of Quasi-3D plasmonic nanostructure arrays with deep and shallow Fabry-Pérot nanocavities *J. Phys. Chem. C* **115** 10996–1002
- [6] Henzie J, Lee M H and Odom T W 2007 Multiscale patterning of plasmonic metamaterials *Nat. Nanotechnol.* **2** 549–54
- [7] Xie H, Li Y, Jin S, Han J and Zhao X 2010 Facile fabrication of 3D-ordered macroporous nanocrystalline Iron oxide films with highly efficient visible light induced photocatalytic activity *J. Phys. Chem. C* **114** 9706–12
- [8] Galisteo-López J F, Ibisate M, Sapienza R, Froufe-Pérez L S, Blanco A and López C 2011 Self-assembled photonic structures *Adv. Mater.* **23** 30–69
- [9] Arpin K A, Mihi A, Johnson H T, Baca A J, Rogers J A, Lewis J A and Braun P V 2010 Multidimensional architectures for functional optical devices *Adv. Mater.* **22** 1084–1101
- [10] Heussler S P, Moser H O and Kalaiselvi S M P 2013 3D deep x-ray lithography for producing a multi-channel Fourier transform interferometer *Microsyst. Technol.* **19** 335–41
- [11] Noda S, Tomoda K, Yamamoto N and Chutinan A 2000 Finer features for functional microdevices *Science* **289** 697–8
- [12] Campbell M, Sharp D N, Harrison M T, Denning R G and Turbereld A J 2000 Fabrication of photonic crystals for the visible spectrum by holographic lithography *Nature* **404** 53
- [13] Jang J H, Ullal C K, Maldovan M, Gorishnyy T, Kooi S, Koh C Y and Thomas E L 2007 3D Micro- and nanostructures via interference lithography *Adv. Funct. Mater.* **17** 3027–41
- [14] Tseng A A, Chen K, Chen C D and Ma K J 2003 Electron beam lithography in nanoscale fabrication: recent development *IEEE Trans. Electron. Packag. Manuf.* **26** 141–9
- [15] Ansari K, Kan J A, Bettiol A A and Watt F 2004 Fabrication of high aspect ratio 100 nm metallic stamps for nanoimprint lithography using proton beam writing *Appl. Phys. Lett.* **85** 476–8
- [16] Wen J J, Shen Z, Qiu Z, Jiang A, Liu R and Chen Y 2011 Fabrication of complex nanostructures of poly(vinylidene fluoride-trifluoroethylene) by dual step hot-embossing *J. Vac. Sci. Technol. B* **29** 1–4
- [17] Odom T W, Love J C, Wolfe D B, Kateri E P and Whitesides G M 2002 Improved pattern transfer in soft lithography using composite stamps *Langmuir* **18** 5314–20
- [18] Kim J, Allen M G and Yoon Y K 2011 Computer-controlled dynamic mode multidirectional UV lithography for 3D microfabrication *J. Micromech. Microeng.* **21** 1–14
- [19] Lee S W and Lee S S 2008 Application of Huygens–Fresnel diffraction principle for high aspect ratio SU8 micro-/nanotip *Opt. Lett.* **33** 40–1
- [20] Zhu Z, Zhou Z, Huang Q-A and Li W-H 2008 Modeling, simulation and experimental verification of inclined UV lithography for SU8 negative thick photoresists *J. Micromech. Microeng.* **18** 1–11
- [21] Gaudet M, Camart J-C, Buchaillet L and Arscott S 2006 Variation of absorption coefficient and determination of critical dose of SU8 at 365 nm *Appl. Phys. Lett.* **88** 1–3